Biointerphases
A Journal of Biomaterials and Biological Interfaces

ARTICLE

avs.scitation.org/journal/bip

Characterizing protein G B1 orientation and its effect on immunoglobulin G antibody binding using XPS, ToF-SIMS, and quartz crystal microbalance with dissipation monitoring

Cite as: Biointerphases 15, 021002 (2020); doi: 10.1116/1.5142560
Submitted: 14 December 2019 · Accepted: 19 February 2020 ·
Published Online: 13 March 2020

Elisa T. Harrison,[1,a)] Yung-Chen Wang,[2,b)] Lauren Carter,[3] and David G. Castner[1,2]

AFFILIATIONS

[1]National ESCA and Surface Analysis Center for Biomedical Problems, Department of Chemical Engineering, University of Washington, Seattle, Washington 98195
[2]National ESCA and Surface Analysis Center for Biomedical Problems, Department of Bioengineering, University of Washington, Seattle, Washington 98195
[3]Institute for Protein Design, Department of Biochemistry, University of Washington, Seattle, Washington 98195

Note: This paper is part of the Special Topic Collection on Quartz Crystal Microbalance in Biological Surface Science and Soft Matter.

[a)]**Present address:** Ford Motor Company, Research and Innovation Center, 2101 Village Road, Room 1337, MD 3182, Dearborn, Michigan 48121.
[b)]**Present address:** Medtronic, Corporate Science and Technology, 710 Medtronic Parkway, Mailstop LT240, Minneapolis, Minnesota 55432.

ABSTRACT

Controlling how proteins are immobilized (e.g., controlling their orientation and conformation) is essential for developing and optimizing the performance of *in vitro* protein-binding devices, such as enzyme-linked immunosorbent assays. Characterizing the identity, orientation, etc., of proteins in complex mixtures of immobilized proteins requires a multitechnique approach. The focus of this work was to control and characterize the orientation of protein G B1, an immunoglobulin G (IgG) antibody-binding domain of protein G, on well-defined surfaces and to measure the effect of protein G B1 orientation on IgG antibody binding. The surface sensitivity of time-of-flight secondary ion mass spectrometry (ToF-SIMS) was used to distinguish between different proteins and their orientation on both flat and nanoparticle gold surfaces by monitoring intensity changes of characteristic amino acid mass fragments. Amino acids distributed asymmetrically were used to calculate peak intensity ratios from ToF-SIMS data to determine the orientation of protein G B1 cysteine mutants covalently attached to a maleimide surface. To study the effect of protein orientation on antibody binding, multilayer protein films on flat gold surfaces were formed by binding IgG to the immobilized protein G B1 films. Quartz crystal microbalance with dissipation monitoring and x-ray photoelectron spectroscopy analysis revealed that coverage and orientation affected the antibody-binding process. At high protein G B1 coverage, the cysteine mutant immobilized in an end-on orientation with the C-terminus exposed bound 443 ng/cm^2 of whole IgG (H + L) antibodies. In comparison, the high coverage cysteine mutant immobilized in an end-on orientation with the N-terminus exposed did not bind detectable amounts of whole IgG (H + L) antibodies.

I. INTRODUCTION

Control of protein immobilization onto surfaces is essential for the development of *in vitro* binding protein devices, such as enzyme-linked immunosorbent assays (ELISA) and protein microarrays.[1,2] Controlled adsorption of proteins onto surfaces, via hydrophobic interactions, electrostatic interactions, or covalent attachment, has been used to improve the antibody-binding capabilities of binding assays. Specifically, the orientation of proteins can play a vital role in the function and performance of such binding assays.[2–7]

The need to control the immobilization of proteins onto surfaces motivates the necessity for developing methods capable of fully analyzing protein-surface interactions. Thus, surface analytical techniques are being developed that provide a more detailed understanding of immobilized proteins. In binding assays, such as sandwich ELISAs, the structure and activity of proteins are typically determined indirectly by measuring how the proteins bind to other proteins and/or antibodies.[8–10] Oftentimes, many layers of proteins and antibodies, along with blocking proteins such as bovine serum albumin, are formed on top of the protein of interest and labels are often required before any information can be gathered. Binding proteins that would otherwise be ruled out because of a lack of signal may, in fact, be useful if researchers could fully control the structure, orientation, and thus the activity of that immobilized protein. To take the empirical trial and error aspect out of the design of diagnostic tools, surface analytical techniques, such as x-ray photoelectron spectroscopy (XPS), quartz crystal microbalance with dissipation monitoring (QCM-D), and time-of-flight secondary ion mass spectrometry (ToF-SIMS), can provide a molecular-level understanding of protein-surface systems, such as composition, mass of adsorbed proteins, orientation, activity, and adsorption/binding kinetics of immobilized proteins.[11–23]

Each of the techniques used in this study has its strengths and weaknesses.[22] XPS can be used in a qualitative mode to identify which elements are present in the surface region to determine if the expected elements are present (i.e., C, N, and O from protein and Au from the substrate) or if unexpected elements are present (e.g., elements from surface contaminates).[18] XPS can also be used in a quantitative mode to determine how much of particular element is present in the surface region.[18] The chemical specificity of XPS is limited. For example, it is straightforward to distinguish protein from gold but not straightforward to distinguish one protein from another protein. Also, XPS analysis is done in ultrahigh vacuum (UHV) and the process of introducing the sample into UHV can change the structure of the sample (e.g., denature proteins). ToF-SIMS is a complementary UHV analysis technique to XPS.[15] Like XPS, it is an analysis technique that can be used in a qualitative mode to identify which elements are present in the surface region. Unlike XPS, it is challenging to use ToF-SIMS in a quantitative manner due to the well-known "matrix effect." The major advantages of ToF-SIMS relative to XPS are its enhanced chemical specificity (e.g., ability to distinguish different proteins), enhanced surface sensitivity when used in the low dose (i.e., static) mode, and lower detection limits. ToF-SIMS's combination of chemical and surface specificity makes it an excellent technique for determining protein conformation and orientation.[1,24] QCM-D is a technique that can quantify changes in mass and viscoelastic properties at the liquid-solid interface[25] but does not have any inherent chemical specificity, making it an ideal complementary analysis technique to XPS and ToF-SIMS. Surface functionalization of the QCM-D sensor [e.g., with self-assembled monolayers (SAMs)] can indirectly provide some level of chemical specificity to QCM-D measurements, but it is best to validate that the desired surface functionalization has been achieved by using techniques such as XPS and ToF-SIMS. Also, indirect information about biomolecule orientation can be obtained from QCM-D measurements, for example, if sufficient antigen binding is detected to a layer of antibodies indicating that the antibodies are oriented with their antigen binding sites available for reaction. Conversely, if no antigen binding is detected, the antibodies could be either be denatured or oriented with their antigen binding site not available for reaction, and other analysis (e.g., with ToF-SIMS) is needed to determine the reason no antigen binding is detected. Thus, combining QCM-D with XPS and ToF-SIMS provides quantitative, real-time binding information directly at the liquid-solution interface from QCM-D that can be interpreted using the chemical and structural information provided by XPS and ToF-SIMS.

Protein G and protein A, due to their specificity in binding to the Fc region of antibodies, are widely used to optimize the antibody orientation in ELISA and protein microarray applications.[9] For protein G B1, the Fc binding site is located near the C-terminus of protein G B1. Thus, for protein G B1 to be effective in orienting antibodies for optimal antigen binding, it must be oriented with its C-terminus exposed and available to bind to the antibody Fc region. So, it is essential to develop the tools and methods that can determine protein G B1 orientation. In this study, we have utilized surface analytical methods to (1) characterize the amounts and orientation of protein G B1 cysteine mutants covalently attached to a maleimide surface, (2) distinguish between protein G B1 and antibodies in multicomponent protein films, and (3) measure the effect of protein G B1 orientation on antibody binding. Protein G B1, a 6 kDa, 56 amino acid immunoglobulin G (IgG) antibody-binding domain of protein G, was used in this study because of its stability, both in solution and immobilized on surfaces, and the availability of experimental data.[13,26–36] SAMs were used to modify the surfaces due to their ease of preparation, precision of surface control, and wide variety of possible surface chemistries.[14,20,37–39] To control orientation, cysteine mutants of protein G B1 were immobilized onto maleimide-oligo (ethylene glycol)-functionalized (MEG) SAMs formed on flat and nanoparticle (NP) gold surfaces. XPS was used to verify the quality of the substrates and to quantify protein adsorption. QCM-D was used to measure changes in mass and viscoelastic properties of immobilized proteins as a function of time for the flat surfaces.[8,20,25,40,41] The orientation of immobilized protein films was determined using ToF-SIMS intensity peak ratio analysis.[1,13,16,26,27,42,43]

Multicomponent protein films were formed using protein G B1 and IgG antibodies adsorbed onto flat gold surfaces. The chemical specificity and increased surface sensitively of ToF-SIMS, especially with the introduction of cluster ion sources,[44–46] was used to distinguish between proteins and antibodies in multicomponent protein films.[16,17,47,48] Additionally, the antibody-binding capabilities of the protein G B1 mutants immobilized onto MEG-covered flat gold surfaces were characterized using QCM-D. This work addresses the challenges in studying complex, multicomponent protein/antibody films by advancing our ability to obtain detailed

information about the structure, orientation, and binding of immobilized proteins and antibodies.

II. MATERIALS AND METHODS

A. Substrate preparation and modification

1. Flat gold surfaces

Gold-coated silicon wafers (used for XPS and ToF-SIMS analysis) and gold-coated quartz crystal sensors (used for QCM-D analysis) were employed as flat substrates for protein immobilization studies. Silicon wafers (Silicon Valley Microelectronics Inc., San Jose, CA) were diced into $1 \times 1\ cm^2$ substrates using a diamond saw and then solvent cleaned. Gold substrates were fabricated by depositing a 5 nm titanium adhesion layer followed by depositing a 100 nm gold layer onto the diced and cleaned silicon substrates via electron-beam evaporation at room temperature and pressures $<1 \times 10^{-6}$ Torr. Gold-coated quartz crystal sensors (Q-Sense, Gothenburg, Sweden) were first treated with an UV-Ozone cleaner and then immersed into a 75 °C heated piranha solution (5:1:1 water:hydrogen peroxide: ammonium hydroxide solution; *caution: piranha solution reacts violently with organic compounds*) prior to surface modification.

The SAM substrates used in this work were prepared by submerging the flat gold-coated substrates in a solution of 1 mM maleimide-oligo(ethylene glycol) (MEG) disulfide (HO-EG4-C11-S-S-C11-EG6-NHCO-Maleimide, Prochimia, Sopot, Poland) in 200-proof ethanol (Fisher Scientific) for at least 16 h. The substrates were then rinsed and sonicated in ethanol to remove unbound molecules. Bare gold-coated substrates used in the protein adsorption experiment were submerged in 200-proof ethanol in a separate hood to minimize thiol or disulfide contamination.

2. Gold nanoparticles

Briefly, 13 nm gold NPs (AuNPs) were synthesized using the citrate reduction method adopted from Frens' study[49] as described previously,[50–52] in which the size of the AuNPs can be readily tuned by adjusting the ratio of gold chloride to sodium citrate during the NP synthesis. Prior to the synthesis of AuNPs, all glassware was cleaned using aqua regia to remove potential residual gold on the glassware from previous syntheses. Reagents used included sodium citrate tribasic dehydrate (Sigma-Aldrich, St. Louis, MO) and gold (III) chloride hydrate (99.999%) (Sigma-Aldrich, St. Louis, MO). AuNPs used in this study were prepared using a 1% (w/v) citrate solution and a 0.01% (w/v) Au solution mixed in a 2.5:100 volumetric ratio.[50] Synthesized AuNPs were sealed and stored at 4 °C.

AuNPs were functionalized with MEG SAMs by exposing the citrate capped AuNPs to 100 uM of MEG in de-ionized (DI) water for 36 h. The MEG functionalized AuNPs were sonicated for 30 s and subsequently purified using three rounds of 9000 rpm/30 min centrifugation-resuspension method to remove excess thiol in solution. To break up the AuNP pellet before each resuspension, the pellet was vortexed for 30 s and sonicated for 1 min.

B. Protein synthesis

Wild type (WT), two cysteine mutants, and charged mutants of protein G B1 have been synthesized and characterized previously.[26,27] The focus of those previous studies was to characterize the orientation of those protein G B1 immobilized on flat surfaces. This study explored new synthesis protocols for expressing additional cysteine mutants, their immobilization onto flat and NP gold surfaces, and their binding capacity for whole IgG (H + L) antibody and IgG $F(ab')_2$ fragment. Both the whole and $F(ab')_2$ fragment antibodies were purchased from Jackson ImmunoResearch (West Grove, PA).

The plasmids for WT protein G B1 and G B1 point mutants were ordered from Genscript in the pet29b vector (Invitrogen). The amino acids chosen for the point mutations were selected based on location, ease of synthesis, and predicted binding site of protein G B1 to the IgG antibody. The WT protein G B1 and point mutant sequences are listed in Table 1 in the supplementary material[61] and their locations in the protein G B1 structure are shown in Fig. 1. The mutants are labeled according to the amino acid that was replaced by cysteine. For example, T11C represents a mutant where cysteine replaced threonine at the 11 position in the sequence. T11C, D36C, and E42C all represent mutations near the protein G B1 C-terminus and V21C and T49C represent mutations near the protein G B1N-terminus.

Upon receipt and verification of sequence, the plasmids were transformed into the Lemo21 *E. coli* expression strain (NEB) using standard heat shock transformation protocol. Transformants were plated on Teknova minimal media containing 0.1% glucose, kanamycin, chloramphenicol, and M9 salts and then incubated overnight at 37 °C. The following day a single colony was inoculated into 50 ml of Luria Broth growth media containing 50 ug/ml kanamycin to maintain selection, and grown overnight at 37 °C with shaking at 225 rpm. After approximately 18 h, the overnight

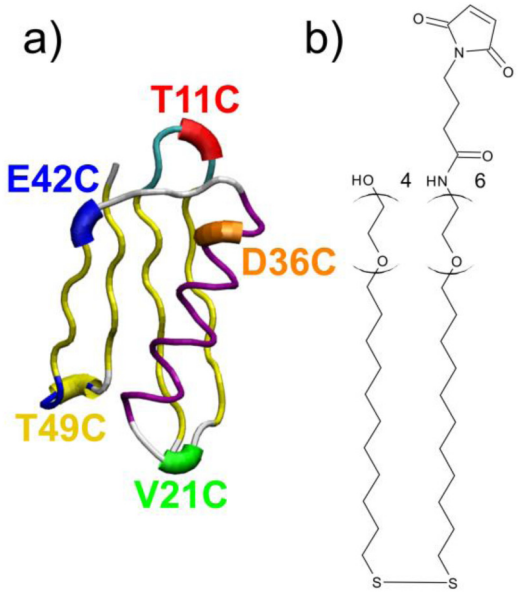

FIG. 1. (a) Location of cysteine point mutations on protein G B1 (T11C, V21C, D36C, E42C, and T49C) will covalently attach to (b) MEG disulfide SAMs.

culture was removed and 10 ml was used to inoculate 0.5 l of Terrific Broth (Difco), containing kanamycin to 50 ug/ml, rhamnose to 1 mM, and 50× M salts to 1× (Studier). The large expression culture was incubated at 37 °C with shaking at 225 rpm until the OD600 reached 0.8, indicating log phase growth. At this time, a sample was removed for SDS-PAGE, and IPTG was added to 1 mM. The temperature was lowered to 20 °C and the culture was incubated overnight at 20 °C with shaking at 225 rpm. After approximately 18 h, the culture was removed and a 1 ml sample was taken for SDS-PAGE analysis. The *E. coli* were pelleted at 4000 rpm for 20 min and the media was discarded. The cell pellet was resuspended with 20 mM Tris 150 mM sodium chloride at pH8 with 25 ml buffer per gram of cell weight.

The resuspended cells were lysed using a Microfluidics M100P microfluidizer at a pressure of 18 000 psi. The lysate was then centrifuged at 17 000 *g* for 30 min to pellet cell debris and insoluble proteins. The clarified soluble supernatant was removed to a new tube and the soluble fraction then subjected to anion exchange chromatography. Chromatography was performed on a GE Healthcare Pure M instrument using a GE Healthcare Q Sepharose Fast Flow resin. The $2.2 \times 10\ cm^2$ column was equilibrated using three column volumes of 20 mM Tris 150 mM NaCl at pH8 and then the soluble fraction was applied to the column. The WT protein G B1 and point mutants were flowed through the column, in the negative mode, with host cell protein and DNA remaining bound. The purified proteins were then dialyzed into a carbonate/bicarbonate buffer at pH9 and analyzed by sodium dodecyl sulfate–polyacrylamide gel electropheresis (SDS-PAGE) for quality, mass spectrometry for identity, and A280 for concentration.

C. Protein immobilization

1. Flat gold surfaces

Protein immobilization was done in a static mode for XPS and ToF-SIMS studies and in a flow mode for QCM-D studies. Protein G B1, whole IgG (H + L) antibody, and IgG $F(ab')_2$ fragment antibody solutions, with concentrations ranging from 50 μg/ml to 1 mg/ml, were prepared in bicarbonate/carbonate buffer (50 mM, pH 9.5). The buffer was degassed and sonicated for an hour prior to use. Substrates used for static protein or antibody immobilization were hydrated in 0.5 ml degassed buffer in a 24-well plate for 30 min at room temperature prior to adding the protein or antibody solution and then allowing the immobilization to occur for 2 h at room temperature. After protein or antibody immobilization, substrates were rinsed by serial dilution in buffer and then submerged in a series of two buffer and three water solutions for 5 min each while mixing with a stir bar. Substrates were then dried and stored under nitrogen gas.

Samples prepared for XPS and ToF-SIMS required drying and exposure to ultrahigh vacuum conditions while samples prepared in the QCM-D were conducted in solution. Substrates were analyzed by XPS and ToF-SIMS within a week of preparation. Replicates were prepared on different days using freshly prepared protein solutions.

2. Gold nanoparticles

AuNPs functionalized with MEG were incubated with 1 mg/ml of protein G B1 WT and mutants in phosphate buffered saline (PBS) overnight at room temperature on a shaker shaking at 200 rpm. To remove excess proteins in solution or proteins that are loosely bound to the surface of the AuNPs, the following purification protocol was used. After overnight incubation with protein, the AuNPs were purified using three rounds of 12 000 rpm/40 min centrifugation-resuspension cycles with PBS. To break up the AuNP pellet before each resuspension, the pellet was vortexed for 30 s and sonicated for 1 min. After the third rinsing cycle, the AuNP solution was transferred to a 1000 kDa dialysis tube (SpectrumLabs, Rancho Dominquez, CA). Dialysis against DI H_2O was performed for two 2-h rinse cycles and one overnight rinse under constant stirring. After the overnight dialysis, the AuNP solution was retrieved and purified by centrifugation at 12 000 rpm for 40 min. After removing the supernatant and backfilling with nitrogen gas, and the concentrated AuNPs were ready for XPS and ToF-SIMS analysis. For sample preparation, AuNPs were deposited onto clean silicon substrate and let dry in a vacuum desiccator. Usually, 10 ul of the AuNP solution was deposited at a time until a confluent layer is formed on the Si wafer to prevent the signal from the substrate being detected during the XPS and ToF-SIMS analysis.

D. X-ray photoelectron spectroscopy

XPS data were acquired with an AxisUltra DLD system (Kratos Analytical, Manchester, England) for the flat surfaces and an S-Probe XPS system (Surface Science Instruments, Mountain View, CA) for the NPs. Both instruments use a monochromatic Al $Ka_{1,2}$ x-ray source ($h\nu = 1486.6$ eV). Elemental compositions were calculated from survey (Au, C, and O) and detailed scans (S and N) collected with analyzer pass energies of either 150 eV (S-probe) or 160 eV (AxisUltra DLD). The survey step size was 1 eV, while 0.4 eV was used for detail scans. High-resolution spectra were acquired with lower analyzer pass energies of 50 eV (S-probe) or 20 eV (AxisUltra DLD). Elemental compositions (atomic percentages) were calculated from the S-probe data using the HAWK DATA ANALYSIS 7 software (Service Physics, Inc., Bend, Oregon) and from the AxisUltra DLD using the CASAXPS software (http://www.casaxps.com/).

E. Quartz crystal microbalance with dissipation monitoring

Adsorption and binding of protein G B1 was monitored using the E4 QCM-D system (Q-Sense, Gothenburg, Sweden). Frequency and dissipation measurements were made on gold-coated quartz crystals with fundamental frequencies of 4.95 MHz (Q-Sense, Gothenburg, Sweden) functionalized with MEG SAMs. Replicates were conducted for each protein, antibody, and substrate combination. The temperature was maintained at 22 °C. During a typical QCM-D experiment, protein G B1 was immobilized onto the sensors at concentrations ranging from 50 to 1000 μg/ml in buffer at a flow rate of 300 μl/min. Following protein G B1 adsorption, the system was rinsed with buffer at 300 μl/min to remove any excess protein. IgG antibodies were then immobilized at a concentration of 50 μg/ml in buffer at a flow rate of 300 μl/min. Again, the system was rinsed with buffer at 300 μl/min to remove unbound antibodies. Additional layers were formed similarly. Prior to the QCM-D experiment, the temperature was stabilized for at least 30 min and the buffer baseline was established for at least 30 min.

F. Time-of-flight secondary ion mass spectrometry

Negative and positive secondary ion spectra from the immobilized protein G B1 samples used to determine protein orientation were acquired on a TOF.SIMS 5–100 instrument (IONTOF, Munster, Germany) using a pulsed 25 keV Bi_3^+ primary ion beam under static conditions (primary ion dose $<10^{12}$ ions/cm^2). Spectra were collected from five $100 \times 100\,\mu m^2$ regions for each sample. Secondary ions were collected over a range of 0–800 m/z at a mass resolution (m/Δm) between 4000 and 8000. Positive spectra m/z values were mass calibrated using CH_3^+, $C_2H_3^+$, and $C_3H_5^+$ peaks, and negative spectra using CH^-, OH^-, C_2H^-, C_3^-, C_4H^-, and C_5^- peaks. Mass calibration errors were typically below 20 ppm.

Positive ion spectra used to analyze protein/antibody multilayers were acquired using a J105 Chemical Imager (Ionoptika, Southhampton, UK) using an argon gas cluster ion beam (GCIB). The GCIB was operated at 40 keV using argon 4000 clusters containing ~15% CO_2 (Matheson Tri-Gas, Fife, Washington). Spectra were collected from a $500 \times 500\,\mu m^2$ area with a dose of $\sim 3.6 \times 10^{11}$ ions/cm^2. The instrument was mass calibrated using peaks at masses m/z 219, 527, and 731 from a thin film of Irganox 1010. Mass calibration errors were below 5 ppm.

G. Principal component analysis

Principal component analysis (PCA) has been described in detail previously.[53] PCA processing of the ToF-SIMS data was done as described previously[27] using a series of scripts written by NESAC/BIO (http://www.nb.uw.edu/mvsa/multivariate-surface-analysis-homepage). A list of all significant positive ion peaks derived only from the protein was compiled based on a database of ToF-SIMS ion fragmentation patterns for all 20 amino acids.[43,47] Any peaks that could originate from both protein and MEG layers were not included in the analysis so that PCA would highlight differences between bound proteins. The datasets were preprocessed by first normalizing to the sum of the selected amino acid peaks. Then, the data were square root transformed and mean-centered.

H. Transmission electron microscopy

The shape and size of the AuNPs were verified using transmission electron microscopy (TEM) analysis. The TEM analysis was done by drying AuNPs directly onto a carbon-supported TEM grid (Ted Pella, Redding, CA). The AuNP solution was produced by centrifuging 1.5 ml of AuNPs under 12 000 rpm for 20 min. After removing the supernatant, the AuNPs were resuspended using 0.5 ml mixture of 50:50 ethanol and DI H_2O. The ethanol solution was used to accelerate the drying process and prevent particle aggregation. TEM images were taken on an FEI Tecnai G2 F20 TEM (FEI, Hillsboro, Oregon) operating with 200 kV acceleration of the electron beam and 180–245kX magnification. All images were taken at a 2048×2048 pixel resolution using the bright field mode. The size and circularity of the AuNPs was analyzed from the TEM images using the particle analysis algorithm in IMAGEJ (version 1.46d, National Institutes of Health, USA).

I. Liquid chromatography mass spectrometry

Protein GB1 samples were analyzed by liquid chromatography mass spectrometry (LCMS) at the University of Washington Mass Spectrometer Facility to verify the correct mass was synthesized. Each protein sample was diluted to concentration of ~10 uM/ml with deionized water and a 2 ml aliquot placed into an autosampler vial used to inject 5 ul of each sample into an HPLC column (Zorbax SB-C18, 2.1×100 mm, Agilent Technologies, Santa Clara, CA). The column eluent was analyzed using the EsquireLC ion trap mass spectrometer (Bruker Daltonics, Billerica, MA) operating in the positive ionization mode. The Agilent 1100 HPLC used solvents A (water 94%, acetonitrile 5%, 1% acetic acid) and B (acetonitrile 99%, 1% acetic acid) and separated peptides using the following gradients: 5% B to 100% B in 10 min, 10–15 min at 100%B and equilibrated at initial conditions for 8 min prior the next injection.

Full mass spectra in the range 200–2200 m/z were collected every second during the LC run. Data were analyzed using software (Bruker Daltonics) that deconvoluted the multiply charged ion spectra to provide the molecular weight of the analyzed peptides.

III. RESULTS AND DISCUSSION

A. Protein synthesis

Previously published protocols produced WT, T11C and V21C cysteine mutants, and a charged mutant of protein G B1 in good yield and purity.[26,27] For this work, we were interested in preparing additional cysteine mutants and explored different protocols to produce these mutants. All protocols examined thus far produced WT protein G B1 in good yields and purity. However, varying degrees of success were observed for the different cysteine mutants. Given the varied success of producing cysteine mutants, all the results reported in this study used protein synthesized and purified using the protocol described in Sec. II B. Additionally, some batch to batch yield variation was observed even when using the same protocol, so all results presented in this study are from the same batch of protein.

For the synthetic protocol used in this study, WT, V21C, and D36C protein G B1 mutants were produced in good yields with correct masses as determined by LCMS. WT was detected as a monomer, while V21C and D36C were detected as dimers, not surprising given the mutants contain cysteine. T49C was obtained in low yield, but with the correct mass. The E42C and T11C mutants synthesized with this protocol did not have correct masses and therefore results from these mutants are not reported.

B. XPS analysis of protein G B1 immobilization

1. Flat gold surfaces

XPS results for the MEG-covered flat gold substrates and the immobilized V21C, D36C, and T49C protein G B1 mutants onto the MEG-covered flat gold substrates (solutions concentrations of ~1 mg/ml) are shown in Table I. For comparison, XPS results of the immobilized mutants onto flat bare gold substrates are also included in Table I.

In Table I, the C, O, N, and S atomic percentages (at. %) were renormalized to 100 at. % to remove the gold (Au) signal and investigate the organic overlayer composition. The gold signal is monitored to access the overlayer thickness and coverage since the gold signal will be attenuated as the overlayer thickness or coverage increases. For protein adsorption, the nitrogen concentration was monitored

TABLE I. XPS elemental compositions for the substrates (flat bare gold and MEG-covered flat gold) and immobilized protein G B1 cysteine mutants (V21C, D36C, and T49C). The XPS-determined elemental compositions of the organic overlayer were calculated by excluding Au signal and renormalizing the remaining signals to 100 at. %. The Au atomic percentages shown are prior to this normalization. The corrected N percentages (N_{att}) represent the protein G B1 contribution to the total nitrogen signal and are calculated prior to removing the Au contribution (n.d. = not detected).

	XPS atomic percent					
	Organic overlayer					
Sample	C	O	N	S	Au	N_{att}
MEG only	69.1 ± 2.1	24.6 ± 2.1	3.3 ± 0.3	3.1 ± 0.5	42.3 ± 3.3	
V21C on MEG	70.2 ± 2.7	20.6 ± 1.5	5.5 ± 1.4	3.7 ± 0.3	31.8 ± 1.7	2.3 ± 0.9
D36C on MEG	72.2 ± 0.7	21.4 ± 1.0	4.1 ± 0.5	2.3 ± 0.7	28.7 ± 2.7	1.6 ± 0.2
T49C on MEG	70.2 ± 2.2	20.8 ± 1.4	5.6 ± 1.0	3.4 ± 0.6	31.9 ± 2.4	2.4 ± 0.8
Bare Au	90.6 ± 2.6	6.2 ± 3.0	n.d.	3.2 ± 0.6	71.9 ± 0.7	
V21C on Au	68.5 ± 2.4	17.9 ± 1.5	11.1 ± 0.7	2.5 ± 0.5	32.9 ± 1.8	
D36C on Au	67.0 ± 2.5	18.5 ± 0.8	12.1 ± 1.2	2.3 ± 0.5	31.5 ± 3.2	
T49C on Au	68.1 ± 0.8	3.0 ± 0.6	10.6 ± 0.2	3.0 ± 0.6	26.9 ± 4.2	
WT on Au	66.7 ± 2.2	18.3 ± 1.4	13.0 ± 0.7	2.1 ± 0.3	23.0 ± 1.4	

since protein (~10–12 at. % N) has a larger nitrogen concentration compared to the MEG SAM (~2 at. % N) or bare gold substrate (no N). Proteins adsorbed onto flat bare gold substrates exhibited N atomic percentages from the organic overlayer of ~12 at. %. This N signal, coupled with the large decrease in the gold signal (from ~72 to ~25–30 at. %), suggests that at least a monolayer of protein G B1 was formed on the bare gold substrate.[19]

Upon protein G B1 immobilization onto the MEG-covered flat gold substrates, the N atomic percentage of the organic overlayer increased from ~3 to ~5 at. %. The smaller increase in N at. % detected on the MEG surfaces compared to the bare gold substrates is consistent with previous results[27] and is likely due to two reasons. First, the N concentration from organic overlayer represents a weighted average of the nitrogen from protein G B1 and MEG. Second, the protein-resistant nature of the ethylene glycol component in MEG could be reducing the amount of protein G B1 immobilized and preventing multilayer and nonspecific protein adsorption.[24] To separate the protein G B1 nitrogen signal from the MEG SAM nitrogen signal, the total nitrogen signal was corrected using the protocol described in Ref. 24. The corrected nitrogen signals, N_{att}, which represent the nitrogen signal from protein G B1 only, are also included in Table I.

WT protein G B1 does not contain cysteine and should have minimal immobilization to MEG SAM substrates.[27] In the current study, the increase in nitrogen atomic percent when MEG-covered flat gold substrates were exposed to WT protein G B1 varied from minimal amounts to amounts approaching those observed for the cysteine mutants. This variation is likely due to nonspecific absorption of WT protein G B1 at pH 9.5, possibly due to partial hydrolysis of the maleimide groups and/or deprotonation of the lysine primary amine groups on the surface of protein G B1. The nonspecific adsorption of WT protein G B1 onto MEG-covered gold surfaces has been observed previously.[27]

2. NP gold surfaces

TEM bright field images and particle analysis for the citrate covered AuNPs in Fig. 1 in the supplementary material[61] showed that they were monodispersed with the average diameter of 12.9 ± 0.9 nm (n = 2417 particles). The AuNPs are spherically shaped with a 1.1 major-axis to minor-axis ratio. No batch-to-batch inconsistencies regarding the circularity and size distribution of the particles were observed.

Table II shows the XPS-determined elemental composition of unfunctionalized (as synthesized), MEG-covered, and protein G B1 WT/mutants immobilized AuNPs. For citrate stabilized AuNPs, the gold signal from the AuNPs and the carbon, oxygen, and sodium signals from the sodium citrate layer were detected. After MEG

TABLE II. XPS elemental composition of unfunctionalized, MEG functionalized, and immobilized protein G B1 on AuNPs (n.d. = not detected).

	XPS atomic percent					
Sample	C	O	N	S	Au	Na
Unfunctionalized	34.6 ± 4.3	15.1 ± 4.4	n.d.	n.d.	46.7 ± 6.3	3.2 ± 1.5
MEG	59.5 ± 1.6	21.4 ± 1.0	2.0 ± 0.7	1.5 ± 0.5	15.7 ± 1.2	n.d.
MEG + WT	65.0 ± 4.5	23.3 ± 2.8	3.7 ± 1.6	0.8 ± 0.7	7.2 ± 4.0	n.d.
MEG + V21C	65.0 ± 1.5	23.1 ± 1.3	6.5 ± 0.7	0.8 ± 0.3	4.6 ± 1.6	n.d.
MEG + D36C	66.3 ± 0.4	20.4 ± 0.5	5.8 ± 0.5	1.0 ± 0.2	6.5 ± 0.4	n.d.
MEG + T49C	61.4 ± 1.4	22.4 ± 1.5	7.1 ± 0.3	1.0 ± 0.2	8.1 ± 0.2	n.d.

SAMs functionalization, nitrogen (2 at. %) and sulfur (1.5 at. %) signals were detected along with a decrease in Au concentration (47–16 at. %) and increases in the C (35–60 at. %) and O (15–21 at. %) concentrations, as expected for the displacement of the citrate layer and its replacement with a thicker MEG layer. After incubation of the MEG-covered AuNPs with protein G B1 WT followed by purification, an increase in the nitrogen signal was observed (2 to ~4 at. %). As mentioned above in Sec. III B 1, this increase in nitrogen signal is likely due to nonspecific adsorption of the WT protein. It is possible that the edge and corner atoms present in AuNPs can also have an impact on the assembly of the MEG SAMs, leading to nonspecific protein adsorption.[54]

Compared to WT protein G B1, all protein G B1 cysteine mutants resulted in significantly larger increase of the nitrogen signal (to ~6–7 at. %). This larger increase in nitrogen signal for the protein G B1 cysteine mutants is consistent with site-specific immobilization through the maleimide-cysteine linkage. The XPS results show that the protein G B1 cysteine mutants can be successfully immobilized onto the AuNPs through maleimide-cysteine coupling. Although the XPS results for protein G B1 immobilization onto MEG-covered flat and NP Au surfaces were similar, some differences were observed. In particular, higher N and lower Au concentrations were detected on the AuNP samples. This is due to the difference in XPS sampling depths of the flat and NP samples. For the flat Au, the XPS data were acquired with the surface oriented 90° to the axis of the analyzer lens, which results in the maximum sampling depth. For the AuNPs, even though the substrate they were deposited onto had its surface oriented 90° to the axis of the analyzer lens, the full range of photoelectron take-off angles was detected from the AuNPs.[50,51] Thus, the sampling depth for XPS analysis of AuNPs was smaller than that for the flat Au surfaces. This results in larger signals from the protein overlayer and smaller signals from the underlying Au from the protein covered AuNPs.

C. QCM-D analysis of protein G B1 immobilization

The mass of protein G B1 immobilized from ~1 mg/ml solutions was calculated with the Sauerbrey equation[55,56] using the change in frequency measured using QCM-D. The Sauerbrey equation can only be used if the dissipation is low. For protein G B1 immobilization onto both MEG SAM and bare flat gold substrates, the change in dissipation remained low compared to the change in frequency (<1%). This suggests that a rigid film of protein G B1 was formed on the two substrates, thus satisfying the requirements for using the Sauerbrey equation. The changes in frequency and dissipation for protein G B1 immobilization onto the MEG-covered flat gold and flat bare gold substrates are listed in Table III.

The QCM-D results correlated well with the XPS results. QCM-D and XPS both show the immobilization of all types of protein G B1 (WT, V21C, D36C, and T49C) formed a thicker film on the bare Au surface compared to the MEG-covered Au surface. On the MEG-covered Au surface, the amount of V21C and D36C immobilized was consistent with the amounts expected for a monolayer of protein G B1 (~100 ng/cm^2). The higher amounts of protein G B1 adsorbed on bare Au suggest formation of a protein multilayer on bare Au surfaces. However, it should be noted that QCM-D measures the "wet" mass, so the total calculated mass includes both the protein and any water associated with it. Also, QCM-D showed the WT protein G B1 adsorbed onto bare Au surfaces in slightly higher amounts compared to the protein G B1 cysteine mutants. This is consistent with the XPS results where WT protein G B1 adsorption on bare Au produced slightly lower Au signals and slightly higher N concentrations compared to the protein G B1 cysteine mutants.

For the MEG-covered flat Au surfaces, the amount of protein G B1 immobilized depended on the type of protein G B1 sample. Both XPS and QCM-D showed that the WT protein G B1 was immobilized in significantly lower amounts compared to the V21C and D36C protein G B1 mutants. XPS analysis showed that the amount of T49C protein G B1 mutant immobilized to the MEG surfaces was similar to the other two cysteine mutants, but the QCM-D analysis showed that it fell between the WT and other two cysteine mutants. The reason for the T49C differences between XPS and QCM-D could be due to low synthesis yield of the T49C, affecting flow immobilization (QCM-D) more than static immobilization (XPS).

To further correlate the XPS and QCM-D results, additional experiments were done with the D36C protein G B1 mutant. The D36C protein G B1 concentration in buffer was varied and the amount of protein immobilized was monitored using QCM-D (Sauerbrey mass) and XPS (corrected nitrogen signal, N_{att}) (see Fig. 2). At the lowest protein concentrations used (50 and 250 μg/ml D36C in buffer solution), the calculated Sauerbrey mass was

TABLE III. Changes in frequency and dissipation along with the calculated Sauerbrey mass for protein G B1 V21C, D36C, and WT immobilization onto the MEG SAM and bare gold substrates. The Sauerbrey mass was calculated from the seventh frequency overtone. The calculated mass includes water associated with the protein film.

Sample	Change in frequency (Hz)	Change in dissipation ($\times 10^{-6}$)	Sauerbrey mass (ng/cm^2)
V21C on MEG/Au	−4.0 ± 0.6	0.3 ± 0.03	70 ± 11
D36C on MEG/Au	−6.3 ± 1.5	0.7 ± 0.1	111 ± 26
T49C on MEG/Au	−2.2 ± 0.1	0.4 ± 0.3	39 ± 1
WT on MEG/Au	−1.5 ± 0.3	0.2 ± 0.01	26 ± 4
V21C on bare Au	−14 ± 1	0.8 ± 0.01	247 ± 14
D36C on bare Au	−20 ± 3	1.8 ± 0.6	343 ± 56
T49C on bare Au	−15 ± 2	1.3 ± 0.3	261 ± 27
WT on bare Au	−24 ± 3	2.5 ± 0.5	420 ± 55

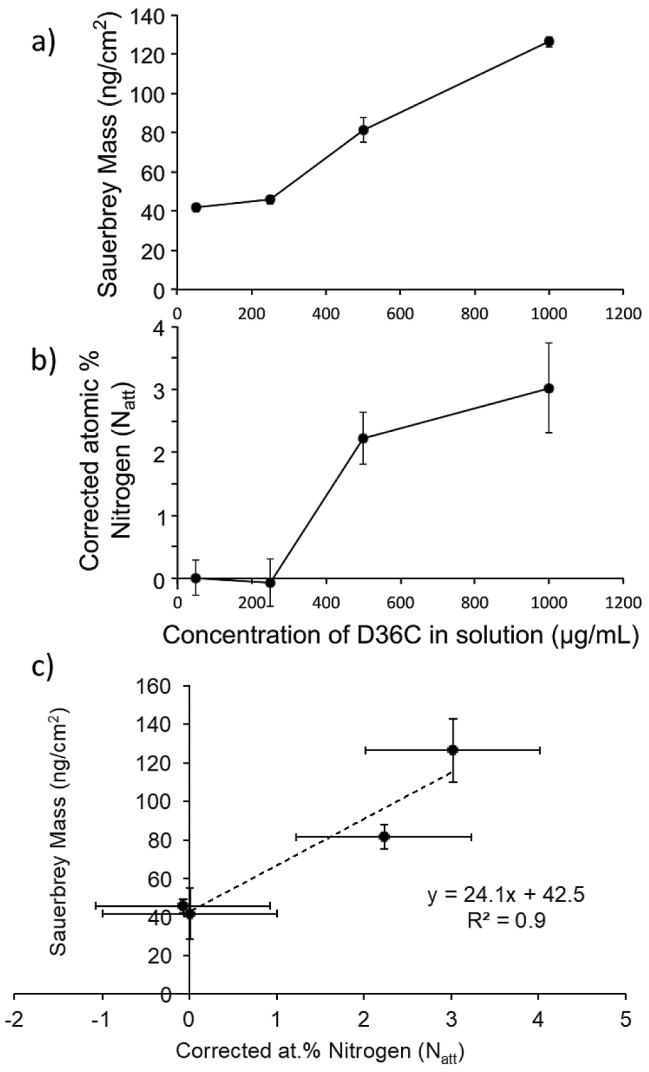

FIG. 2. Concentration isotherms of the D36C cysteine mutant of protein G B1 to compare changes in composition measured using QCM-D (calculated Sauerbrey mass) (a) and XPS (N_{att}) (b). Correlation between the XPS corrected atomic percentage of nitrogen and the QCM-D calculated Sauerbrey mass for immobilization of protein G B1 D36C cysteine mutant onto the MEG SAM substrates (c).

~40 ng/cm^2 and only trace amounts of nitrogen were detected by XPS. Both N_{att} and the Sauerbrey mass increased as the D36C solution concentration was increased from 250 to 1000 μg/ml. We would expect the curves to eventually level off as the protein solution is increased above 1000 μg/ml; however, the risk of aggregation in solution increases as the protein concentration increases, so no experiments at solution concentrations above 1000 μg/ml were performed.

The correlation between the corrected atomic percentage of nitrogen (N_{att}) and the calculated Sauerbrey mass for D36C protein G B1 mutant immobilization onto MEG-covered Au substrates is shown in Fig. 2(c). A similar linear trend is obtained when the corrected atomic percentage of nitrogen and the calculated Sauerbrey mass for all protein G B1 cysteine mutants are included in the same plot (Fig. 2 in the supplementary material[61]). It should be noted that the corrected nitrogen atomic percentage and the Sauerbrey mass were only correlated if the same protein solution was used for both XPS and QCM-D experiments since the concentration of the protein solution was shown to affect the amount of protein immobilized. It should also be noted that ~40 ng/cm^2 of protein immobilization was detected by QCM-D when the XPS N_{att} was ~0. Part of this difference is likely due to QCM-D measuring a wet mass (amount of protein immobilized plus any change in water content) while XPS measures a dry mass (just protein) since XPS measurements are made in ultrahigh vacuum. Also, the presence of nitrogen in the MEG SAM will affect the XPS detection limits[57] but not the QCM-D detection limits.

Additionally, the effect of hydrolysis of the maleimide group on protein G B1 immobilization was investigated using the D36C protein G B1 mutant. For these experiments, the MEG-covered Au substrates were first submerged in pure buffer for 0.5, 1, 3, and 17 h. These hydrated MEG-covered Au substrates were then dried using nitrogen and placed in the QCM-D flow modules for immobilization experiments. The changes in frequency, dissipation, and calculated Sauerbrey mass for the D36C protein G B1 mutant after maleimide hydrolysis are shown in Fig. 3. Using a 1000 μg/ml solution of D36C protein G B1, the calculated Sauerbrey mass decreased to 61 ng/cm^2 after 30 min of buffer soaking and to 31 ng/cm^2 after 3 h of buffer soaking (note these buffer soak times are in addition to the normal 30-min buffer exposure used to equilibrate the QCM-D flow cell for protein immobilization experiments). These amounts are significantly lower than the ~100 ng/cm^2 of D36C protein G B1 immobilized without soaking in buffer prior to the protein immobilization experiments (see Table III). The calculated Sauerbrey mass after both the 3 and 17-h buffer exposure was at the minimum amount detected in the lowest protein concentrations in previous experiments

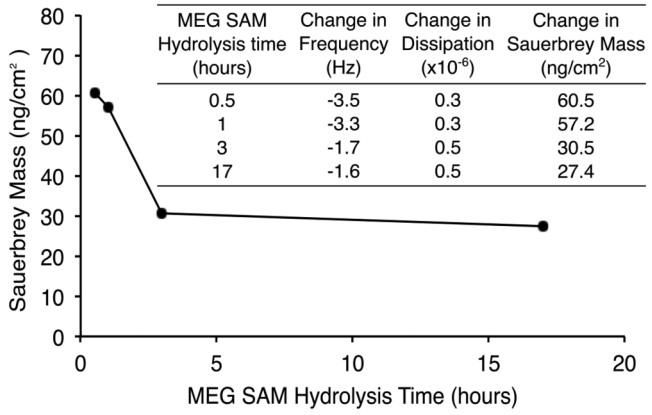

MEG SAM Hydrolysis time (hours)	Change in Frequency (Hz)	Change in Dissipation (x10^{-6})	Change in Sauerbrey Mass (ng/cm^2)
0.5	-3.5	0.3	60.5
1	-3.3	0.3	57.2
3	-1.7	0.5	30.5
17	-1.6	0.5	27.4

FIG. 3. Calculated Sauerbrey mass (from the QCM-D 7th frequency overtone) with varying hydrolysis times of the MEG-covered Au substrate prior to D36C protein G B1 mutant immobilization. Inset shows the observed changes in frequency and dissipation.

(~40 ng/cm^2). These experiments show that significant hydrolysis of the maleimide groups in the pH 9.5 buffer solution can occur within 30 min.

D. ToF-SIMS analysis of protein G B1 orientation

The orientation of immobilized protein films can be determined using ToF-SIMS.[1,13,16,26,27,42,43] ToF-SIMS peak ratio analysis using mass fragments asymmetrically distributed in the protein G B1 3D structure to determine protein G B1 orientation on the MEG-covered surfaces is shown in Fig. 4. The ratio was calculated from the intensity of mass fragments produced with a Bi_3^+ primary ion beam from amino acids Ile/Leu, Gly, Asn, and Tyr. Figure 4(a) lists the amino acids, the mass of the characteristic amino acid ion fragments, and a visualization of the amino acid distribution in the crystal structure as using visual molecular dynamics (VMD). Ile/Leu, Gly, and Asn are located near the C-terminus of protein G B1, while Tyr is located near the N-terminus. Protein G B1 immobilized onto MEG-covered surfaces from solution concentrations of ~1 mg/ml was used for the ToF-SIMS peak ratio analysis to achieve approximately monolayer coverage of the proteins.

Orientation peak intensity ratios were calculated as the sum of intensities of amino acid fragments from the C-terminus (Ile/Leu: 86.10; Gly: 85.04, 113.04; Asn: 88.04, 98.02) divided by the sum of intensities of amino acid fragments from the N-terminus (Tyr: 55.02, 107.05). These peak ratios for the D36C and V21C protein G B1 mutants are shown in Fig. 4(b) for the MEG-covered flat Au surfaces and Fig. 4(c) for the MEG-covered AuNP surfaces. Similar to the results shown in Refs. 13, 26, and 27, the peak ratio was higher for the V21C protein G B1 mutant compared to the D36C protein G B1 mutant on both the flat and NP MEG-covered surfaces (Fig. 4). This was expected since the cysteine in the V21C mutant is located opposite the C-terminus while the cysteine in the D36C mutant is located opposite the N-terminus. Although the trends are the same for both the flat and NP surfaces, the absolute values of the peak ratios from the two types of surfaces are different. This is likely due to the different structure of the two MEG surfaces (flat versus spherical).

a)

	C-terminus			N-terminus
Amino Acid:	Ile/Leu	Gly	Asn	Tyr
Mass of ion fragments (m/z):	86.10	85.04 113.04	88.04 98.02	55.02 107.05

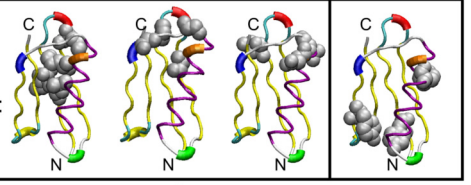

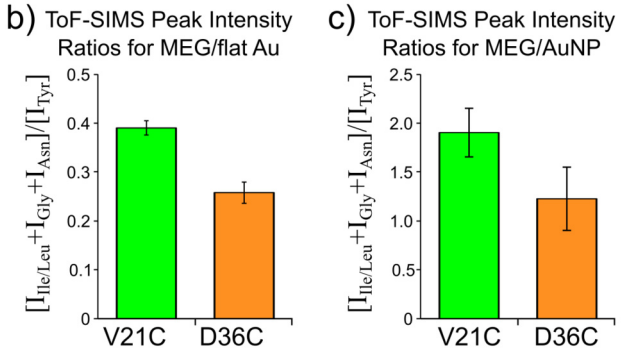

FIG. 4. (a) Amino acids with asymmetric distributions used to calculate ToF-SIMS peak intensity ratios are listed with their characteristic mass fragments and location in the protein G B1 crystal structure highlighted. ToF-SIMS peak intensity ratios for the sum of amino acid fragment intensities from the C-terminus divided by the sum of amino acid fragment intensities from the N-terminus ($[I_{Ile/Leu}+I_{Gly}+I_{Asn}]/[I_{Tyr}]$) for (b) MEG/flat Au and (c) MEG/AuNP surfaces.

E. Formation of multicomponent protein G B1/antibody films

Multicomponent protein films, using the D36C protein G B1 cysteine mutant and IgG antibodies (both whole (H + L) and $F(ab')_2$ fragments), were formed on bare gold substrates. To distinguish between the different species, each component was either immobilized individually or in a sequential fashion [1st: D36C protein G B1 on bare Au substrates; 2nd: whole IgG (H + L) antibody on D36C protein G B1 on bare Au substrates; and 3rd: IgG $F(ab')_2$ fragment antibody on whole IgG (H + L) antibody on D36C protein G B1 on bare Au substrates]. The final multicomponent protein film is shown as an idealized cartoon in Fig. 5. In reality, protein G B1 cysteine mutants are not likely perfectly oriented on the bare Au surface, especially given that QCM-D detects greater than monolayer coverage for all protein G B1 samples adsorbed onto bare gold substrates. In fact, for the D36C protein G B1 mutant, if all molecules were oriented with all cysteines bound to the bare gold surface, the antibody-binding region of protein G B1 would be buried at the gold-D36C interface resulting in no binding of IgG to the D36C protein G B1 film. However, if the

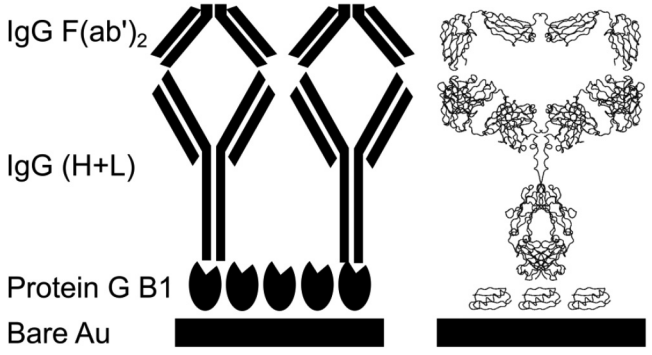

FIG. 5. Idealized cartoon depicting formation of a protein multilayer film from sequential immobilization of protein G B1, whole IgG (H + L), and IgG $F(ab')_2$ fragments onto a bare gold substrate. The multicomponent protein/antibody films are depicted as a cartoon and using the crystal structures of the proteins and antibodies visualized using VMD (Refs. 15 and 36).

TABLE IV. XPS elemental composition of bare gold substrate and immobilized D36C protein G B1, whole IgG (H + L) on D36C protein G B1, and IgG F(ab′)$_2$ fragment antibody on whole IgG (H + L) on D36C protein G B1 on bare gold substrates. The Au signal was normalized out to show the elemental composition of the organic overlayer. The remaining signals, excluding Au, was renormalized to 100%. The Au atomic percentages shown are prior to normalization. The Au signal is monitored to access the overlayer thickness and coverage since the gold signal will be attenuated as the thickness or coverage increases. For protein adsorption, the atomic percentage of N1s was monitored since it is present in protein and not present in the bare gold substrate.

	XPS atomic percent				
	Organic overlayer				
Sample	C	O	N	S	Au
Bare gold	84.9 ± 6.8	15.1 ± 6.8	n.d.	n.d.	76.5 ± 2.3
One layer	69.4 ± 1.3	18.1 ± 1.6	8.5 ± 0.4	4.0 ± 0.2	53.6 ± 1.0
Two layers	67.5 ± 3.6	18.5 ± 3.4	10.3 ± 0.3	3.6 ± 0.3	50.2 ± 1.5
Three layers	65.3 ± 1.1	19.4 ± 0.7	13.0 ± 0.3	2.3 ± 0.5	40.8 ± 1.4

D36C protein G B1 molecules are not perfectly oriented on the bare Au surface, then a small portion of the D36C protein G B1 molecules could have their antibody-binding sites available for binding IgG molecules. Using D36C protein G B1 to form the first layer in the multicomponent protein films thus will minimize the amount of whole IgG and IgG F(ab′)$_2$ immobilized in the second and third steps. This situation will represent the most challenging test for XPS and ToF-SIMS to detect changes in the multicomponent protein film.

1. XPS analysis of multicomponent protein G B1/antibody films

The XPS-determined elemental compositions for the bare gold substrate and each stage of forming the sequential multicomponent protein/antibody film are listed in Table IV. An adventitious hydrocarbon overlayer was detected on the bare gold substrates since the substrates were exposed to the laboratory environment before introduction into ultrahigh vacuum chamber of the XPS instrument.[58] With each species added to the multicomponent protein/antibody film, the measured nitrogen signal increased and the gold signal decreased due to the increasing the thickness of the multicomponent protein film. Note that the largest decrease in the gold signal was observed for the formation of the first layer (adsorption of D36C protein G B1). Even though the size of D36C protein G B1 is significantly smaller than IgG, only a minimal decrease in the gold signal was detected from the two-component film (IgG + D36C protein G B1) compared to the one-component film (D36C protein G B1). This observation is consistent with only a small fraction of the D36C protein G B1 film having their antibody-binding site at the surface of the film and available to bind IgG.

2. ToF-SIMS analysis of multicomponent protein G B1/antibody films

XPS is useful for quantifying amounts of proteins immobilized onto surfaces by determining the elemental composition of the top 10 nm of the substrate.[14–16,18,19] However, it is extremely challenging for XPS to distinguish between layers of different proteins and antibodies since they contain similar amino acids and elemental chemical compositions. In addition, the sampling depth of XPS can encompass multiple protein layers. The increased surface sensitivity of ToF-SIMS with large gas cluster ion beams was used to detect slight differences in the intensities of characteristic amino acid mass fragments among the different proteins.[16,17,47,59] PCA was used to reduce the dimensions of the ToF-SIMS data.[16,47,53] For proteins immobilized both individually and in a sequential assembly, PCA identified spectral differences between D36C protein G B1, whole IgG (H + L) antibodies, and IgG F(ab′)$_2$ fragment antibodies using protein-only characteristic amino acid mass fragments. The PCA results are shown in Fig. 6.

For proteins and antibodies immobilized individually and sequentially on bare gold substrates, principal component one (PC1) captured 70%–90% of the variance in the amino acid only fragments.[17,42,60] The highest loading peaks in Figs. 6(b) and 6(d) were similar whether the proteins and antibodies were immobilized individually or sequentially, with Trp, Arg, Pro, and Val amino acid peaks loading positively and Ala, Met, Glu amino acid peaks loading negatively. Since protein G B1 had negative PC1 scores, amino acids that have a higher percentage in the sequence of the IgG antibodies [whole (H + L) and F(ab′)$_2$ fragment] are expected to load positively and amino acids with a higher percentage in the sequence of protein G B1 are expected to load negatively. Two amino acids are not present in protein G B1 (Pro and Arg), which explains the high positive loading Pro and Arg characteristic peaks. To explain the remaining high loading amino acid peaks, the amino acid compositions of the proteins and antibodies were investigated. The numbers and percentages of each amino acid in the sequence of the proteins and antibodies are listed in Table 2 in the supplementary material.[61]

Amino acid fragments of Ala, Glu, and Met are among the highest negatively loading amino acid fragments. These three amino acids combined are responsible for 22% of PGB1 sequence compared to only 10% of IgG (H + L) and 14% of IgG F(ab′)$_2$. On the other hand, amino acid fragments of Pro, Arg, Val, and Trp are among the highest positively loading amino acid fragments. These three amino acids combined are responsible for only 9% of the PGB1 sequence, compared to 22% in IgG (H + L) and 18% in IgG F(ab′)$_2$. The amino acid compositions differences between protein G B1 and the two IgG antibodies [whole and F(ab′)$_2$] can account for the separation of protein G B1 from the two IgG antibodies in PC1 scores plot. Even though the amino acid composition of the whole IgG and F(ab′)$_2$) fragment are similar, these two antibodies are separated in the PC1 scores plot for both the individual and sequential immobilized antibodies. This suggests that some differences in the immobilized conformation or 3D distribution are responsible for the separation of whole IgG from the F(ab′)$_2$) fragment in the PC1 scores plot.

3. QCM-D analysis of multicomponent protein G B1/antibody films

QCM-D was used to determine the effects of protein G B1 orientation on IgG binding, using both IgG antibodies [both whole (H + L) and F(ab′)$_2$ fragments]. The change in frequency and dissipation was monitored for protein G B1 immobilization onto MEG

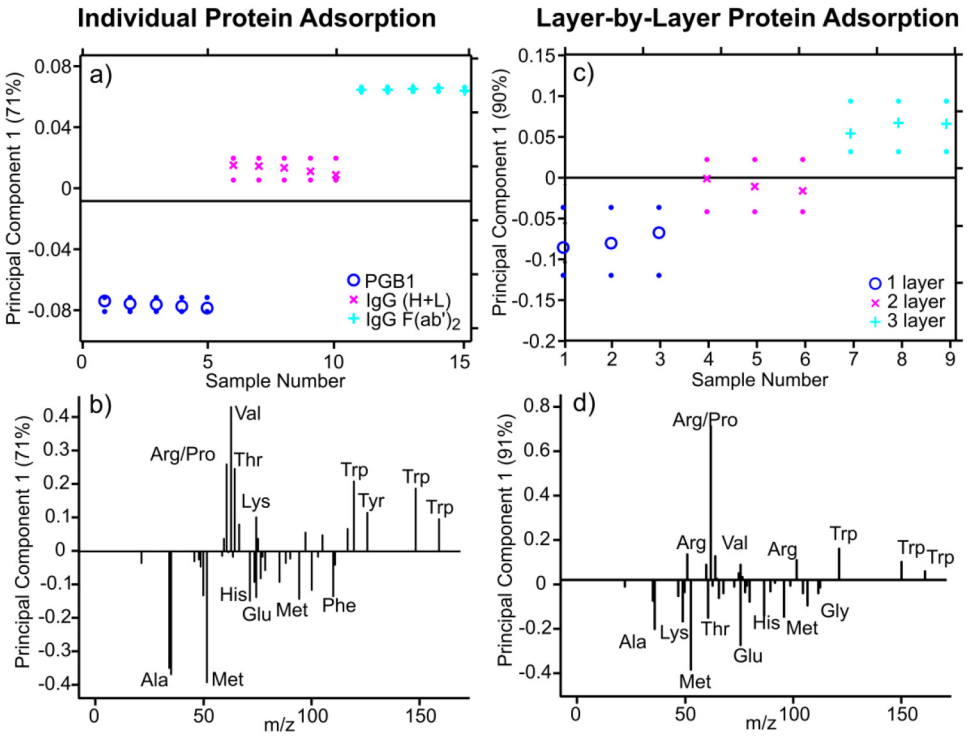

FIG. 6. PCA results for positive ion ToF-SIMS data from the adsorption of [(a) and (b)] individual D36C protein G B1 (PGB1), whole IgG (H + L), and IgG F(ab′)$_2$ fragment onto bare gold substrates and [(c) and (d)] sequential immobilization of PGB1 (1st), whole IgG (H + L) (2nd), and IgG F(ab′)$_2$ fragment (3rd) onto bare gold substrates. PC1 scores [(a) and (c)] and loadings [(b) and (d)] were generated from a set of protein-only peaks and separated PGB1, whole IgG (H + L), and IgG F (ab′)$_2$ fragment both when the proteins were adsorbed individually and when the proteins were sequentially immobilized.

SAM substrates from both high (1 mg/ml) and low (250–500 μg/ml) concentration solutions followed by the sequential binding of whole (H + L) IgG antibodies (100 μg/ml) and F(ab′)$_2$ IgG fragments (100 μg/ml). The results for the amounts of V21C, D36C, and WT protein G B1 immobilized, as well as the amounts of IgG and F (ab′)$_2$ bound to those protein G B1 samples, are shown in Table V. As described in Sec. III C, sufficient amounts of T49C could not be immobilized onto the MEG substrates due to the low synthesis

TABLE V. Change in frequency and dissipation and the calculated Sauerbrey mass for the sequential immobilization of (1) high coverage V21C, D36C, and WT protein G B1 on MEG-covered Au substrates, (2) whole (H + L) IgG antibodies, and (3) F(ab′)$_2$ IgG fragments.

Sample	Change in frequency (Hz)	Change in dissipation ($\times 10^{-6}$)	Change in Sauerbrey mass (ng/cm^2)
V21C, low coverage, on MEG	−3.5	0.3	61.9
+ IgG (H + L)	−4.4	0.4	76.6
+ IgG F(ab′)$_2$	−0.9	0.1	15.3
V21C, high coverage, on MEG	−4.4	0.3	77.3
+ IgG (H + L)	−25.2	1.2	443
+ IgG F(ab′)$_2$	−3.2	0.3	56.4
D36C, low coverage, on MEG	−2.6	0.5	45.7
+ IgG (H + L)	−0.5	0.1	8.7
+ IgG F(ab′)$_2$	−1.7	0.2	29.0
D36C, high coverage, on MEG	−4.6	0.6	81.4
+ IgG (H + L)	0.0	0.0	−0.2
+ IgG F(ab′)$_2$	−0.5	0.0	9.1
WT, low coverage, on MEG	−1.5	0.2	26.4
+ IgG (H + L)	−0.2	0.1	4.1
+ IgG F(ab′)$_2$	−0.5	0.04	8.5
WT, high coverage, on MEG	−1.8	0.8	31.9
+ IgG (H + L)	−2.4	0.3	42.1
+ IgG F(ab′)$_2$	−0.4	0.0	6.6

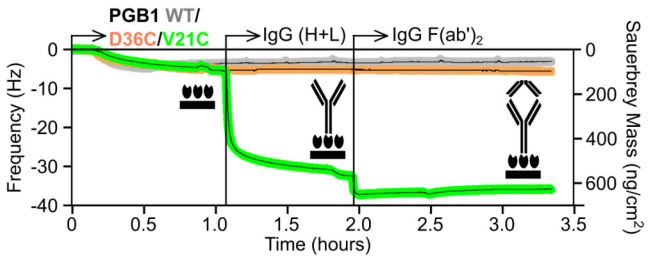

FIG. 7. Changes in frequency and Sauerbrey mass as a function of time during the immobilization of V21C, D36C, and WT protein G B1 onto an MEG SAM surface followed by the sequential binding of whole IgG (H + L) antibody and IgG $F(ab')_2$ fragment antibody. Each immobilization step in the process was followed by a buffer rinse.

yield of T49C. Thus, the T49C results are not included in Table V. The mass attached, in ng/cm^2, was calculated from the seventh overtone after a buffer rinse at each stage in the immobilization process using the Sauerbrey equation.[55,56]

The protein G B1 samples prepared from the high concentration (1 mg/ml) solutions showed the largest differences in IgG binding, indicating that high surface coverage of protein G B1 is important for optimizing the orientation dependence of the protein G B1 mutants. For example, 77 ng/cm^2 of V21C protein G B1 bound 443 ng/cm^2 of whole IgG (H + L) and 56 ng/cm^2 of $F(ab')_2$. This is consistent with the ToF-SIMS results that suggest an end-on orientation of V21C protein G B1 with the C-terminus exposed and the antibody-binding site available to bind whole IgG (H + L) antibodies. In contrast, for similar amounts of D36C protein G B1 (81 ng/cm^2), no detectable amounts of whole IgG (H + L) and only minimal amounts of $F(ab')_2$ (9 ng/cm^2) were observed to bind. This is consistent with the ToF-SIMS results that suggest end-on orientation with the N-terminus exposed which prevents whole IgG (H + L) antibody binding. While the IgG binding results for lower coverage V21C and D36C protein G B1 films showed similar trends, the magnitude of the differences was noticeably smaller than that observed for the corresponding high coverage films. For V21C protein G B1, the amount of IgG binding increased from 77 to 443 ng/cm^2 upon increasing the V21C protein G B1 coverage, while for D36C protein G B1, the amount of IgG binding decreased from 9 ng/cm^2 to not detectable upon increasing the D36C protein G B1 coverage. The QCM-D traces for IgG and $F(ab')_2$ binding to high coverage V21C and D36C protein G B1 films are shown in Fig. 7.

The mass of whole IgG (H + L) antibody bound to the high coverage D36C protein G B1 film (443 ng/cm^2) was ~5× higher than the amount of either D36C or V21C protein G B1 immobilized onto the MEG-covered substrate (~80 ng/cm^2), consistent with the fact that IgG has a significantly higher molecular weight than protein G B1. Note that, regardless of the solution concentrations, only ~30 ng/cm^2 of WT protein G B1 was bound on the MEG surface, resulting in <45 ng/cm^2 of IgG binding to those surfaces. This suggests that in the absence of a well oriented protein G B1 film, small amounts of WT protein G B1 and IgG can attach nonspecifically to the MEG surface.

IV. CONCLUSIONS

Methods to immobilize protein G B1 cysteine mutants onto MEG-covered gold substrates were developed to control the accessibility of the protein G B1 antibody-binding sites. In this work, XPS, QCM-D, and ToF-SIMS were used to characterize the orientation of different protein G B1 cysteine mutants covalently attached to an MEG-covered gold substrate. Control of the accessibility of the antibody-binding sites on the protein was demonstrated by measuring the amount of IgG antibody bound to the protein G B1 cysteine mutants. Controlling the orientation of immobilized proteins can ultimately aid in the development and optimization of *in vitro* binding protein devices, such as enzyme-linked immunosorbent assays.

The following conclusions can be drawn from this work:

(1) V21C, D36C, T49C, and WT protein G B1 were successfully synthesized and their interactions with MEG SAM-covered flat gold and AuNP surfaces as well as flat bare gold substrates were determined using XPS, ToF-SIMS, and QCM-D.
(2) For the protein G B1 cysteine mutants immobilized onto flat MEG-covered gold substrates, the XPS nitrogen atomic percentage, corrected by removing the nitrogen contribution from the MEG SAM substrate, was linearly correlated to the Sauerbrey mass calculated from the QCM-D.
(3) The maleimide group on the MEG SAM is susceptible to hydrolysis and extended exposure to buffer must be avoided to maximize protein G B1 cysteine mutant immobilization.
(4) The surface sensitivity of ToF-SIMS was used to determine protein orientation by monitoring the changes in intensity of characteristic amino acid mass fragments located asymmetrically at the C-terminus and N-terminus of protein G B1. On both the MEG-covered flat and NP gold substrates, D36C protein G B1 preferentially oriented with the N-terminus exposed and the V21C protein G B1 preferentially oriented with the C-terminus exposed.
(5) The orientation of protein G B1 cysteine mutants immobilized onto MEG-covered Au substrates had significant effects on IgG antibody binding. The high coverage V21C protein G B1 film bound 443 ng/cm^2 of IgG compared to no detectable binding of IgG to the high coverage D36C protein G B1 film.
(6) XPS results for sequential formation of multicomponent protein films by immobilizing protein G B1, whole IgG (H + L) antibodies, and IgG $F(ab')_2$ fragment antibodies showed that the nitrogen signal increased, and the gold signal decreased with the addition of each layer due to the increasing the thickness of the organic overlayer.
(7) The surface sensitivity of ToF-SIMS enabled us to distinguish between proteins and antibodies using PCA processing of the ToF-SIMS data.

ACKNOWLEDGMENTS

Recombinant protein G B1 used in this work was obtained from the Institute for Protein Design, University of Washington, Seattle, WA. This study was supported by the National Institutes of Health (NIH) under Grant Nos. P41EB002027 (NESAC/BIO) and S10OD012309. Y.-C. Wang was supported by the National Science Foundation (NSF) Graduate Research Fellowship Program under

Grant No. DGE-1256082. Any opinions, findings, and conclusions or recommendations expressed in this material are those of the author (s) and do not necessarily reflect the views of the NSF or the NIH. Part of this work was conducted at the Molecular Analysis Facility, a National Nanotechnology Coordinated Infrastructure site at the University of Washington, which is supported in part by the NSF under Grant No. NNCI-1542101, the University of Washington, the Molecular Engineering & Sciences Institute, and the Clean Energy Institute. Dan Graham is thanked for his technical expertise and assistance with the ToF-SIMS/PCA of the multicomponent protein G B1/IgG antibody films. Martin Sadilek is thanked for his technical expertise and assistance with the LCMS experiments.

REFERENCES

[1]H. Wang, D. G. Castner, B. D. Ratner, and S. Jiang, Langmuir **20**, 1877 (2004).
[2]P. Peluso *et al.*, Anal. Biochem. **312**, 113 (2003).
[3]E. T. Den Braber, J. E. De Ruijter, L. A. Ginsel, A. F. Von Recum, and J. A. Jansen, J. Biomed. Mater. Res. **40**, 291 (1998).
[4]P. L. Edmiston, J. E. Lee, S.-S. Cheng, and S. S. Saavedra, J. Am. Chem. Soc. **119**, 560 (1997).
[5]T.-W. Cha, A. Guo, and X-Y Zhu, Proteomics **5**, 416 (2005).
[6]J. Turkova, J. Chromatogr. B. **722**, 11 (1999).
[7]S. Kanno, Y. Yanagida, T. Haruyama, E. Kobatake, and M. Aizawa, J. Biotechnol. **76**, 207 (2000).
[8]X. Pei, B. Zhang, J. Tang, B. Liu, W. Lai, and D. Tang, Anal. Chim. Acta **758**, 1 (2013).
[9]P. Wu, D. G. Castner, and D. W. Grainger, J. Biomat. Sci. Polym. E **19**, 725 (2008).
[10]N. G. Welch, J. A. Scoble, B. W. Muir, and P. J. Pigram, Biointerphases **12**, 02D301 (2017).
[11]M. F. Delcroix, S. Demoustier-Champagne, and C. C. Dupont-Gillain, Langmuir **30**, 268 (2013).
[12]F. Fang, J. Satulovsky, and I. Szleifer, Biophys. J. **89**, 1516 (2005).
[13]J. E. Baio, T. Weidner, N. T. Samuel, K. McCrea, L. Baugh, P. S. Stayton, and D. G. Castner, J. Vac. Sci. Technol. B **28**, C5D1 (2010).
[14]F. Cheng, L. J. Gamble, and D. G. Castner, Anal. Chem. **80**, 2564 (2008).
[15]R. N. Foster, E. T. Harrison, and D. G. Castner, Langmuir **32**, 3207 (2016).
[16]J. B. Lhoest, M. S. Wagner, C. D. Tidwell, and D. G. Castner, J. Biomed. Mater. Res. **57**, 432 (2001).
[17]S. Muramoto, D. J. Graham, M. S. Wagner, T. G. Lee, D. W. Moon, and D. G. Castner, J. Phys. Chem. C **115**, 24247 (2011).
[18]S. L. McArthur, Surf. Interface Anal. **38**, 1380 (2006).
[19]R. W. Paynter, B. D. Ratner, T. A. Horbett, and H. R. Thomas, J. Colloid Interface Sci. **101**, 233 (1984).
[20]H. T. M. Phan, S. Bartelt-Hunt, K. B. Rodenhausen, M. Schubert, and J. C. Bartz, PloS One **10**, e0141282 (2015).
[21]K. T. O'Neil, R. H. Hoess, and Daniel P Raleigh, Proteins **21**, 11 (1995).
[22]D. G. Castner, Biointerphases **12**, 02C301 (2017).
[23]D. G. Castner, Surf. Interface Anal. **50**, 981 (2018).
[24]R. Michel, S. Pasche, M. Textor, and D. G. Castner, Langmuir **21**, 12327 (2005).
[25]M. Rodahl, F. Hook, A. Krozer, P. Brzezinski, and B. Kasemo, Rev. Sci. Instrum. **66**, 3924 (1995).
[26]J. E. Baio, T. Weidner, L. Baugh, L. J. Gamble, P. S. Stayton, and D. G. Castner, Langmuir **28**, 2107 (2011).
[27]L. Baugh, T. Weidner, J. E. Baio, P.-C. T. Nguyen, L. J. Gamble, P. S. Stayton, and D. G. Castner, Langmuir **26**, 16434 (2010).
[28]F. J. Blanco, A. R. Ortiz, and L. Serrano, Fold. Des. **2**, 123 (1997).
[29]F. J. Blanco and L. Serrano, Eur. J. Biochem. **230**, 634 (1995).
[30]H.-P. Chiu, B. Kokona, R. Fairman, and R. P. Cheng, J. Am. Chem. Soc. **131**, 13192 (2009).
[31]R. M. Fesinmeyer, F. M. Hudson, and N. H. Andersen, J. Am. Chem. Soc. **126**, 7238 (2004).
[32]V. A. Goehlert, E. Krupinska, L. Regan, and M. J. Stone, Protein Sci. **13**, 3322 (2004).
[33]J. Liu, C. Liao, and J. Zhou, Langmuir **29**, 11366 (2013).
[34]D. J. Sloan and H. W. Hellinga, Protein Sci. **8**, 1643 (1999).
[35]M. J. Stone, S. Gupta, N. Snyder, and L. Regan, J. Am. Chem. Soc. **123**, 185 (2001).
[36]E. T. Harrison, T. Weidner, D. G. Castner, and G. Interlandi, Biointerphases **12**, 2D401 (2017).
[37]E. Cooper and G. J. Leggett, Langmuir **14**, 4795 (1998).
[38]L. Li, S. Chen, and S. Jiang, Langmuir **19**, 2974 (2003).
[39]C.-Y. Lee, P.-C. T. Nguyen, D. W. Grainger, L. J. Gamble, and D. G. Castner, Anal. Chem. **79**, 4390 (2007).
[40]A. Dolatshahi-Pirouz, K. Rechendorff, M. B. Hovgaard, M. Foss, J. Chevallier, and F. Besenbacher, Colloid. Surf. B **66**, 53 (2008).
[41]D. Costa, P-A Garrain, and M. Baaden, J. Biomed. Mater. Res. A **101**, 1210 (2013).
[42]H. E. Canavan, D. J. Graham, X. Cheng, B. D. Ratner, and D. G. Castner, Langmuir **23**, 50 (2007).
[43]D. S. Mantus, B. D. Ratner, B. A. Carlson, and J. F. Moulder, Anal. Chem. **65**, 1431 (1993).
[44]S. Rabbani, A. M. Barber, J. S. Fletcher, N. P. Lockyer, and J. C. Vickerman, Anal. Chem. **83**, 3793 (2011).
[45]D. Rading, R. Moellers, H-G Cramer, and E. Niehuis, Surf. Interface Anal. **45**, 171 (2013).
[46]I. Yamada, J. Matsuo, N. Toyoda, and A. Kirkpatrick, Mater. Sci. Eng. R **34**, 231 (2001).
[47]M. S. Wagner and D. G. Castner, Langmuir **17**, 4649 (2001).
[48]M. S. Wagner, T. A. Horbett, and D. G. Castner, Langmuir **19**, 1708 (2003).
[49]G. Frens, Nat. Phys. Sci. **241**, 20 (1973).
[50]S. D. Techane, Lara J. Gamble, and D. G. Castner, J. Phys. Chem. C **115**, 9432 (2011).
[51]S. D. Techane, D. R. Baer, and D. G. Castner, Anal. Chem. **83**, 6704 (2011).
[52]A. Rafati, A. G. Shard, and D. G. Castner, Biointerphases **11**, 04B304 (2016).
[53]D. J. Graham and D. G. Castner, Biointerphases **7**, 49 (2012).
[54]W. Jiang, B. Y. S. Kim, J. T. Rutka, and W. C. W. Chan, Nat. Nanotechnol. **3**, 145 (2008).
[55]G. Z. Sauerbrey, J. Phys. **155**, 206 (1959).
[56]J. Kankare, Langmuir **18**, 7092 (2002).
[57]M. S. Wagner, S. L. McArthur, M. Shen, T. A. Horbett, and D. G. Castner, J. Biomat. Sci. Polym. E **13**, 407 (2002).
[58]G. C. Smith, J. Rlectron. Spectrosc. **148**, 21 (2005).
[59]M. Dubey, J. Brison, D. W. Grainger, and D. G. Castner, Surf. Interface Anal. **43**, 261 (2011).
[60]M. S. Wagner and D. G. Castner, Appl. Surf. Sci. **231**, 366 (2004).
[61]See supplementary material at https://doi.org/10.1116/1.5142560 for information about Protein G B1 sequences, TEM images of AuNPs, XPS vs QCM-D correlation for all Protein G mutants, and protein amino acid compositions.